

## Proof-of-Principle Experiment for Nanoparticle-Assisted Laser Wakefield Electron Acceleration

Constantin Aniculaesei,<sup>1</sup> Vishwa Bandhu Pathak,<sup>1</sup> Kyung Hwan Oh,<sup>1</sup> Prashant Kumar Singh,<sup>1</sup> Bo Ram Lee,<sup>1</sup> Calin Ioan Hojbota,<sup>1,2</sup> Tae Gyu Pak,<sup>1,2</sup> Enrico Brunetti,<sup>3</sup> Byung Ju Yoo,<sup>1</sup> Jae Hee Sung,<sup>1,4</sup> Seong Ku Lee,<sup>1,4</sup> Hyung Taek Kim<sup>1,4,\*</sup>, and Chang Hee Nam<sup>1,2</sup>

<sup>1</sup>*Center for Relativistic Laser Science, Institute for Basic Science (IBS), Gwangju 61005, Republic of Korea*

<sup>2</sup>*Department of Physics and Photon Science, GIST, Gwangju 61005, Republic of Korea*

<sup>3</sup>*Department of Physics, Scottish Universities Physics Alliance, University of Strathclyde, Glasgow G4 0NG, United Kingdom*

<sup>4</sup>*Advanced Photonics Research Institute, Gwangju Institute of Science and Technology (GIST), Gwangju 61005, Republic of Korea*

(Received 20 June 2019; revised manuscript received 30 July 2019; published 17 October 2019)

Laser electron accelerators have paved the way to build compact electron accelerators, but the quality of the electron beam should be improved to enable efficient use in various specialized applications. We demonstrate a proof-of-principle experiment for nanoparticle-assisted laser wakefield acceleration (NA LWFA) to improve the quality of the electron beam. Nanoparticles are generated through laser ablation of an aluminum target and introduced into a helium plasma to trigger the injection of electrons into the nonlinear plasma wake excited by 70 TW femtosecond laser pulses. We observe a significant enhancement of the electron beam energy, energy spread, and divergence compared with the case of self-injection. For instance, the best quality electron bunches present a maximum energy of up to 340 MeV, with a relative energy spread of 4.7% and a vertical divergence of 5.9 mrad. The initial results on NA LWFA are very promising and motivate further theoretical and experimental research into developing nanoparticle-assisted laser wakefield acceleration.

DOI: 10.1103/PhysRevApplied.12.044041

### I. INTRODUCTION

A laser wakefield accelerator [1] (LWFA) uses the plasma wave generated from the interaction between a high power laser and a plasma to accelerate electrons to relativistic energies. Such unconventional particle accelerators can provide ultrashort relativistic electron beams with potential applications in X-ray free-electron lasers [1,2], biomedical applications [3], radiology, and nuclear medicine [4]. For these applications, LWFA, however, has to be significantly improved in shot-to-shot beam-parameter fluctuations, energy spread, and beam emittance. In the highly nonlinear case of laser-plasma interaction called the “bubble” [5] or “blowout” [6] regime, an intense laser pulse pushes plasma electrons forward and sideways, leaving behind a spherical region (bubble) filled with ions. The displaced electrons form a sheath around the bubble to create an acceleration wakefield that exceeds 100 GV/m. Some of the electrons that cross the base of the bubble can be injected into the bubble in a process called wave breaking [7], or can be injected

into an evolving bubble [8]. The condition for electron self-injection is that the electron group velocity is greater than the phase velocity of the back of the bubble [9]. Electron injection continues until the space-charge effect of the injected electrons is strong enough to stop further injection. Due to the highly nonlinear evolution of the plasma wave, the onset of self-injection depends on the initial conditions of the laser pulse and the plasma medium, leading to some degree of randomness in the self-injection process and, thus, affecting the parameters of the accelerated electron bunch. To overcome the randomness of the injection process, various schemes have been developed or proposed to manipulate the longitudinal momentum of the electrons surrounding the plasma wake [10,11] or the phase velocity of the plasma wake [12,13], or to control the position of particle injection in the wakefield by either using ionization injection [14,15] or an external transverse magnetic field [16].

There have been theoretical studies on the use of a nanowire or nanoparticle for seeding electrons in LWFA. The use of a nanowire in the bubble regime was proposed by Shen *et al.* [17] in 2007, and the use of a nanoparticle was investigated extensively in 2018 by Cho

\*htkim@gist.ac.kr

*et al.* [18] through multidimensional particle-in-cell (PIC) simulations. These new electron acceleration schemes use a nanowire or a nanoparticle to trigger the injection of electrons in the acceleration phase of a plasma wake. A nanoparticle or nanowire is ionized by the leading edge of a laser pulse to create a strong electric field that attracts electrons from the plasma. The attracted electrons can gain additional momentum in the electric field of an ionized nanoparticle and are injected into the bubble. These theoretical studies predict that the characteristics of accelerated beams depend on the nanoparticle composition, size, or number and the moment or position when the nanoparticle is injected into the bubble. The composition or size of the nanoparticle controls the number of electrons injected in the wake and, thus, the charge of the accelerated bunch. The number of nanoparticles controls the number of electron bunches injected into the wake; thus controlling the bunch length, structure, and total charge. Injecting electrons at earlier or later times leads to accurate control of the electron beam energy by increasing the acceleration length and ensuring that injection can happen when the strength of the accelerating field of the wake is highest. Consequently, nanowire- or nanoparticle-assisted laser wakefield acceleration (NA LWFA) could be a versatile scheme due to its high degree of control over the wakefield acceleration process.

Since this kind of scheme was first proposed more than 12 years ago, there have been no experimental attempts to test the viability of NA LWFA. For best performance, the NA LWFA scheme requires an aerodynamic lens system [19] (ALS) that delivers a stream of nanoparticles, which can be injected [18], ideally one nanoparticle at the time,

into the plasma wake with micrometer precision. An ALS is not only bulky and expensive, but also requires serious engineering efforts to integrate it with a gas target.

We investigate the feasibility of a simplified NA LWFA scheme without employing an ALS device. As a source of nanoparticles, we use laser ablation [20], and we integrate it with a supersonic gas jet. This alternative scheme lacks the possibility of controlling the position where a nanoparticle is injected in the plasma wake, but the nanoparticle size and number can be controlled [21] by tuning the fluence of the laser beam used for ablating material. The nanoparticle + helium gas mixture then supersonically expands in a vacuum chamber, interacts with a high power femtosecond laser, and generates an electron beam. In the present case, the ablation laser fluence is reduced until the density of nanoparticles is, theoretically, low enough to assume that the main laser interacts only with a few nanoparticles. The reduction of the laser fluence is achieved while monitoring the electron beam parameters. The results obtained from this proof-of-principle NA LWFA experiment are presented, followed by a brief discussion regarding some aspects of electron injection in the plasma wake in the presence of a nanoparticle.

## II. EXPERIMENTAL RESULTS

The experiment is performed with a 5 Hz Ti:sapphire laser that delivers 1.8 J of energy with 27 fs pulse duration; the setup is shown in Fig. 1. The setup, which is installed in a vacuum chamber that maintains a pressure of  $10^{-5}$  mbar before opening the gas valve, consists of a high-power laser, focusing optics, gas nozzle, and electron beam

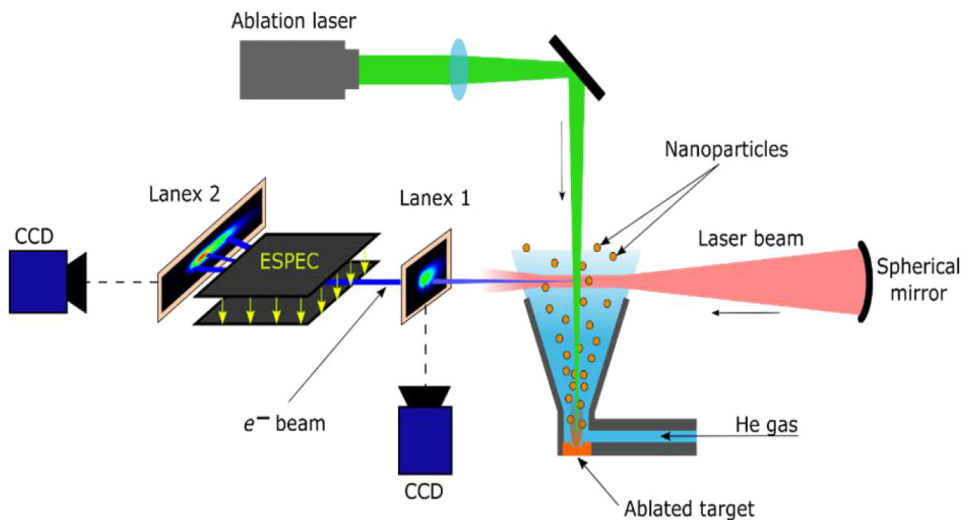


FIG. 1. Experimental setup for nanoparticle-assisted laser wakefield acceleration. The nanoparticles generated through laser ablation mix with helium gas and copropagate towards the outlet region, where the high-power laser excites nonlinear electron plasma waves in the bubble or blowout regime. The density of nanoparticles is estimated to be  $10^7$ – $10^8$  particles/cm $^3$ . Accelerated electron bunches are diagnosed using Lanex™ 1 (transverse profile, pointing, divergence, and charge) and ESPEC + Lanex 2 (energy and energy spread) (ESPEC, electron spectrometer; CCD, charge-coupled device).

diagnostics. The setup is further described in detail in the Appendix. The accelerated electron beam is characterized in terms of vertical and horizontal divergence, peak energy, and relative energy spread. The peak energy is defined as the electron energy where the spectrum presents the highest spectral charge density. All shots are obtained for a helium pressure of 10.5 bar at the nozzle inlet, which corresponds to a measured plasma density of  $5 \times 10^{18} \text{ cm}^{-3}$  at a distance of 1.5 mm above the nozzle. The main laser is focused on the beginning part of the gas jet density ramp at a fixed height of 1.5 mm above the nozzle. These settings are chosen after a systematic scanning of experimental parameters until the most stable electron beam is obtained with helium gas. When used, the ablation laser pulse arrives 10  $\mu\text{s}$  before the main pulse; the delay is empirically set after systematic scanning until the best quality electron beam is obtained through nanoparticle-assisted electron injection. The formation of nanoparticles by an ablation laser is examined by deposition of the nanoparticles on a plate, as shown in the Appendix.

We record two data sets, with and without nanoparticles present in the helium gas jet. From each dataset, we select the best (smallest energy spread) 10 shots, as displayed in Figs. 2 and 3. A summary of the results is shown in Table I. In the case of LWFA with electron self-injection, the quality of the electron beam is very poor, with a relative energy spread, shown in Fig. 2(a), larger than 30% and divergence, shown in Fig. 3(a), larger than 12 mrad. A significant enhancement in electron beam quality is obtained when nanoparticles trigger electron injection. In this case, the relative energy spread, shown in Fig. 2(b), is as small as 4.5%, while the divergence, shown in Fig. 2(b), decreases to 6 mrad. Most of the shots recorded with nanoparticles share the same specific signature: low divergence, spatially well-defined electron bunches, and higher peak

energy with very low energy spread. The nanoparticle source is switched on and off and it is easy to observe that the electron beam quality depends on the presence of the nanoparticles. A small number of shots (about 10% of the total number of 74 shots) have very poor quality, which may be due to the main laser pulse missing the nanoparticles. This is possible because the number of nanoparticles in the volume defined by the laser spot size and gas length, according to theoretical calculations (see Appendix), is very small and estimated to be between 10 and 100 nanoparticles.

In addition, initial tests (not shown here) are performed with higher ablation laser energy (50 mJ), which should increase the number of generated nanoparticles significantly, and it is observed that the generated electron beam has a significant increase in charge and energy spread (more than 100%). We conclude, in this case, that injection occurs due to multiple electron injection from many nanoparticles. Then, with a reduced fluence of the ablation laser, where only a few nanoparticles can be exposed in the laser beam path, we obtain an electron beam with a narrow energy spread. This result is consistent with the conclusions of the theoretical investigation of Cho *et al.* [18].

The peak electron energy recorded with nanoparticles is consistently higher than the case obtained with self-injection. This result could be due to two reasons: space-charge effects [22,23] and acceleration length. As shown in Table I, the electron charge in the case of nanoparticle injection is much smaller than that obtained with self-injection. Since the charge loaded into the bubble modifies locally the acceleration field of the plasma wake, the smaller charge results in a higher effective acceleration field. Another factor that determines the final energy is the distance over which the electrons are accelerated (the

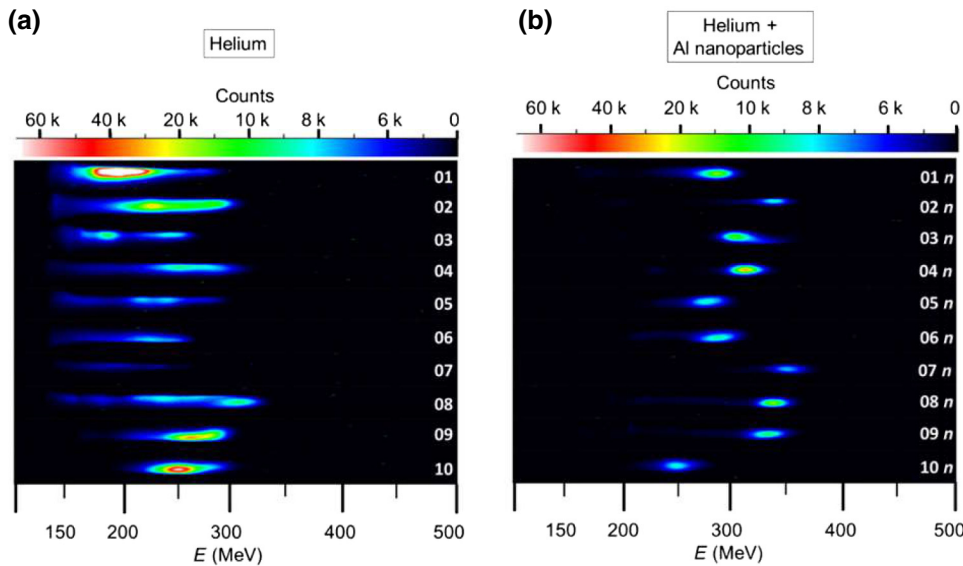


FIG. 2. False-color images of electron energy spectra recorded in the electron spectrometer on Lanex 2. (a) Electron spectra generated without the assistance from nanoparticles and (b) energy spectra generated with nanoparticles. When nanoparticles are used to control electron injection into the bubble, the electron energy spread is significantly reduced, as compared with the case without nanoparticles.

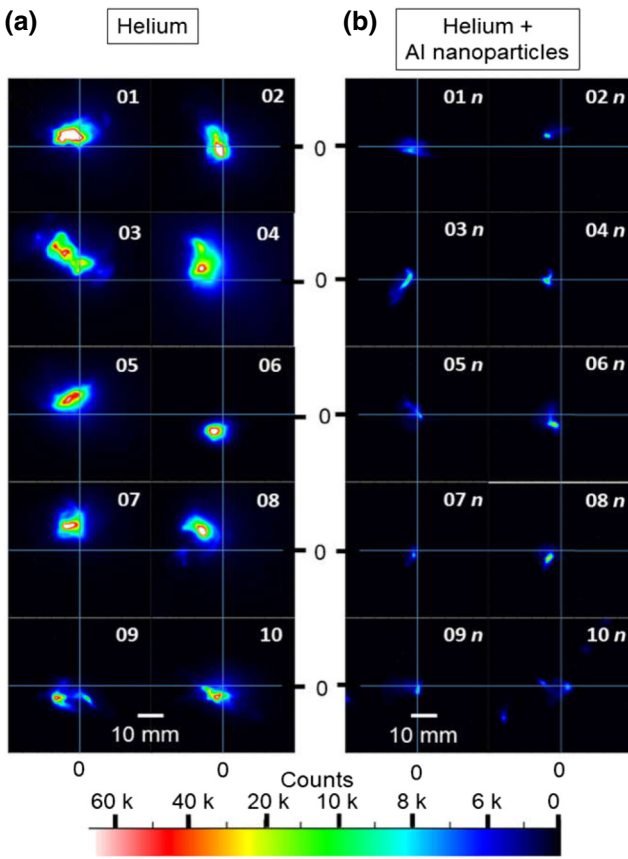


FIG. 3. False-color images of the electron beam distribution recorded with Lanex 1. (a) Electron beam profiles obtained without nanoparticles and (b) electron beam profiles obtained with nanoparticles. When nanoparticles are used, the electron beam divergence is significantly reduced, as compared with the case without nanoparticles.

acceleration length). Three-dimensional PIC simulations, not shown here, using the real experimental parameters indicate that electron self-injection happens almost at the end of the gas jet. In contrast, in the case of NA LWFA, electron injection happens as soon as the plasma wake encounters an ionized nanoparticle. Since the nanoparticles are assumed to be uniformly distributed in the volume of the gas jet, it is very probable that nanoparticle-triggered electron injection could happen at much earlier time than that of the self-injection case, leading to a much longer acceleration length.

The origin of the low divergence in the case of NA LWFA can have multiple causes. The space-charge effect of the injected electron bunch can affect the efficiency of focusing forces inside the bubble; thus, a lower injected charge could mean better control of the bunch in the phase space. In addition, electrons surrounding the nanoparticle occupy a very small volume compared with the volume occupied by electrons that self-inject into the bubble.

Consequently, this leads to smaller divergence of the electron beam from a NA LWFA.

### III. PIC SIMULATIONS

For an insight into the process of electron injection via NA LWFA [17,18], we run two-dimensional PIC simulations using OSIRIS [24]. Details about the simulations can be found in the Appendix. Figure 4 shows the time evolution of plasma density (a1)–(f1) and longitudinal momentum in phase space (a2)–(f2), to clarify the role of nanoparticles in injection. As the laser pulse propagates through the preionized plasma, it pushes background plasma electrons away from the axis, exciting a nonlinear space-charge field, also referred as the wakefield, just behind the laser pulse due to immobile ions [Fig. 4(a1)]. When the laser encounters a preionized and charge-neutral nanoparticle, it pushes nanoparticle electrons away from the axis and excites a very localized space-charge field that grows much stronger than the wakefield, as the rising edge of the laser pulse passes through it [Figs. 4(a2)–4(c2)]; thus, imparting extra momentum to electrons in the vicinity of the laser pulse [Fig. 4(c2)]. As the nanoparticle approaches the trailing edge of the pulse, the field strength of the laser decreases. Consequently, electrons near the nanoparticle, irrespective of origin (background plasma or nanoparticle), are trapped in the nanoparticle potential and travel with the nanoparticle as it passes through the nonlinear wakefield [Fig. 4(d2)]. As the nanoparticle approaches the back of the wakefield [Fig. 4(e2)], the effective field around the nanoparticle again changes in the presence of the strong plasma sheath created by the crossing of background plasma electrons. This triggers the release of electrons into the wakefield of electrons trapped in the potential of the nanoparticle [Figs. 4(e2) and 4(f2)]. It is necessary to mention here that only the outer periphery of the nanoparticle, where the nanoparticle potential is comparable to the ponderomotive or wakefield potential, is the region from which the trapped electrons are injected at the backside of the wakefield. The electron dynamics in the core region of the nanoparticle remains unaffected by the ponderomotive or wakefield potential.

The interaction between the nanoparticle and the laser, shown in Figs. 4(b1)–4(f1), also triggers transverse plasma modulations [17] initially at the front of the laser pulse. Plasma electrons in this region, due to snow-ploughing effect [25], stay in the front part of the laser on a longer timescale. The transverse modulation, thus, also stays with the laser, extending, at the same time, to the whole wakefield region and evolving transversely. These density modulations can strongly diffract the laser pulse. This may explain why successive random self-injection is not observed experimentally, in the presence of nanoparticles. In our simulations, we do not observe any injection caused by the transverse density modulation, as reported

TABLE I. Summarized electron beam parameters for the selected shots shown in Figs. 2 and 3. The shot number with suffix “n” corresponds to the data taken in the presence of nanoparticles. RMS, root-mean-square.

No shot	RMS peak energy (MeV)	RMS energy spread (%)	RMS horizontal divergence (mrad)	RMS vertical divergence (mrad)	Relative charge (arb. units)
01	187	31.5	22.1	9.3	29.2
02	139	71.9	26.1	12.5	21.1
03	215	141.8	13.2	16.0	25.6
04	174	27.5	27.2	18.4	42.5
05	247	64.7	20.6	23.1	23.4
06	182	64.2	23.9	12.3	8.3
07	192	60.9	11.7	7.2	18.5
08	178	37.6	17.2	12.3	20.0
09	235	77.4	19.1	11.0	4.6
10	202	49.5	18.2	31.8	7.8
01n	275	9.0	12.1	9.3	1.6
02n	338	4.7	8.1	5.7	0.6
03n	306	6.4	6.9	7.0	1.3
04n	312	5.4	5.3	4.1	0.7
05n	276	8.2	8.2	6.9	0.8
06n	286	7.9	6.2	6.1	1.2
07n	344	5.5	5.8	6.4	0.3
08n	338	4.5	7.1	5.9	0.9
09n	331	6.0	20.0	6.4	0.8
10n	248	8.9	23.3	16.1	1.1

by Shen *et al.* [17]. The experimental results presented here show that the nanoparticle-assisted injection scheme for LWFA produces much better quality beams than that of the self-injection case. We, however, do not claim that self-injection always generates poor-quality electron beams. Results in the literature show that good-quality electron beams can be obtained using the self-injection scheme [26–29], but the exact laser parameters are not yet fully identified. Here, the improvement of the electron beam quality is caused by localized electron injection with a nanoparticle and trimming successive random self-injections.

#### IV. DISCUSSION

We observe that the insertion of the nanoparticle can significantly reduce the energy spread and divergence of the accelerated electron beam. However, in the experiment, the self-injection case initially produced very poor quality electron beams. For instance, during the experiment, we measure strong nanosecond laser prepulses of the order of  $10^{-4}$ , relative to the main pulse, and their effect on the wakefield acceleration is not yet quantified. The presence of the prepulse could also lead to Coulomb explosion of the nanoparticle [17], but this effect, even if present, does not seem to affect the quality of most electron bunches. Further investigation will be required to clarify this aspect of the experiment. Even under conditions that make electron self-injection very hard to achieve, nanoparticle-assisted electron injection significantly enhances the electron beam

quality. This proof-of-principle experiment of NA LWFA can be further improved using the same setup presented here, but with a more stable laser. This should enhance the shot-to-shot stability of electron beams; thus permitting a systematic scan of more experimental configurations, such as the use of a femtosecond ablation laser or different ablated material.

The results presented in this work could have merit for the development of femtosecond laser wakefield accelerators operating at kHz repletion rates [30]. In high repetition rate LWFA, technology constraints currently limit the laser energy to a few tens of mJ; thus requiring high-density small-length gas targets to produce an electron beam. Since the ablation laser can be operated with a kHz repetition rate, the application of nanoparticle-assisted LWFA, more easily than that of other injection methods with magnetic field or plasma density variations, can be promptly developed with a kHz repetition rate. The use of nanoparticle-assisted electron injection can boost the electron energy and significantly improve the beam quality; thus opening the way towards the development of a wide range of applications of kHz mJ laser wakefield accelerators.

This work proves that NA LWFA is a viable scheme. It is worthwhile investing time, effort, and money to integrate an ALS with a gas target to allow better control of the charge, energy, energy spread, and bunch structure of the accelerated electron beam. Especially, the ALS system for NA LWFA can be an excellent electron injector for obtaining a tens of GeV electron beam with multi-PW lasers. To increase electron energy, plasma density should

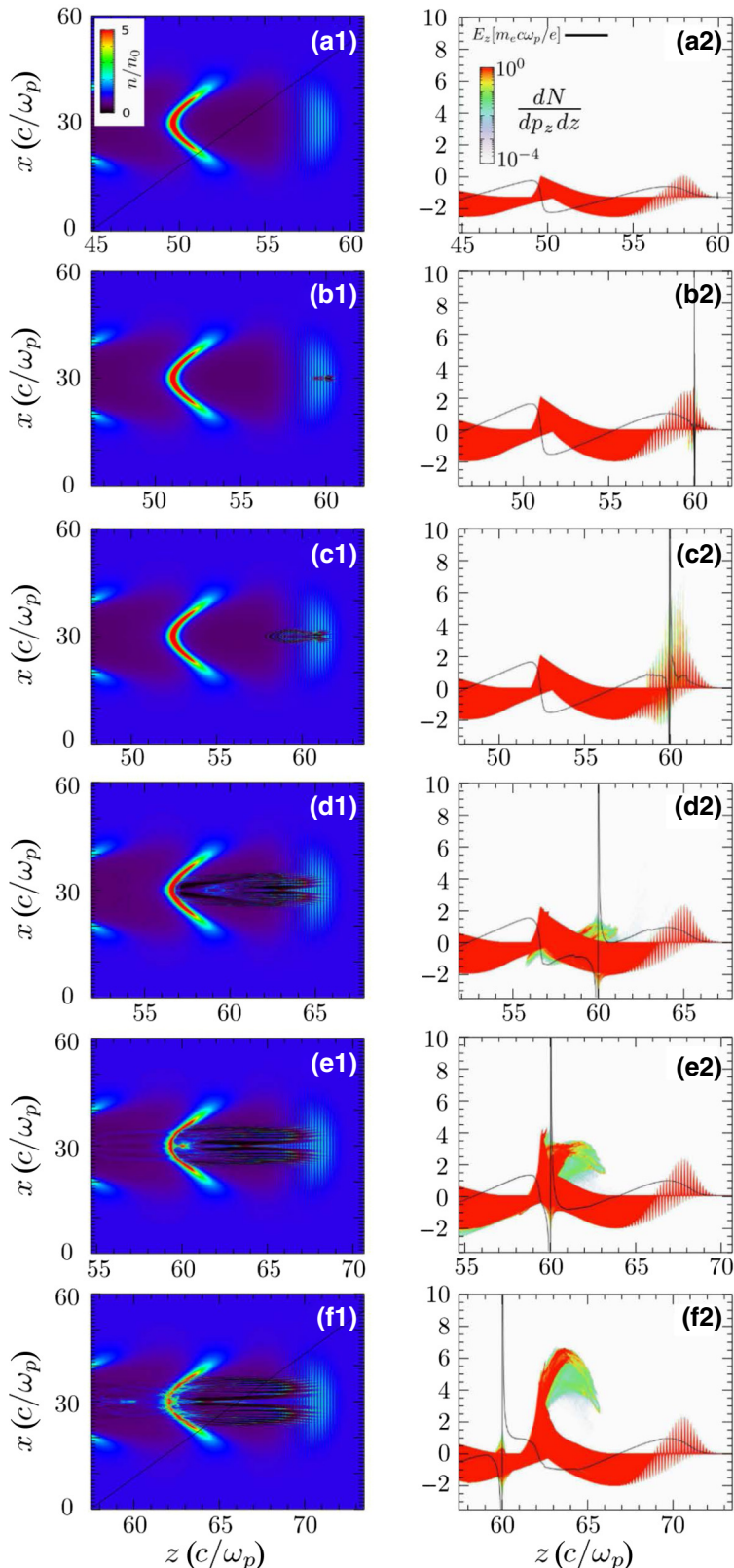


FIG. 4. 2D PIC simulations highlighting the nanoparticle-assisted trapping of plasma electrons in the nonlinear wakefield excited by a laser. (a1)–(f1) Snapshots of plasma density profiles at progressing times, and (a2)–(f2) corresponding phase-space diagrams. The solid lines in (a2)–(f2) are the on-axis longitudinal fields, and the spikes in the fields are due to the nanoparticle space charge. A fully ionized 20 nm nanoparticle, with  $100n_{cr}$  charge density, is initialized at  $z = 60c/\omega_p$ , and the window moves with velocity  $c$  following the laser pulse.

be extremely low so that can interrupt self-injection process. On the other hand, the low density of the medium can be helpful to build the ALS system due to the ease of differential pumping. Thus, the ALS system mounted in a long gas medium with low density can realize a high-quality electron injector for LWFA with multi-PW lasers. In addition, the nanoparticle-assisted LWFA is a versatile method to control the characteristics of the electron beam. We can control the characteristics of the accelerated electron beam by choosing the position, size, density, species, and shape of the nanoparticles. Thus, we can develop laser electron accelerators with a required specification by controlling the nanoparticle parameters.

Finally, it is worth mentioning that localized electron injection in the NA LWFA can produce an electron bunch with extraordinarily short length. Our 2D PIC simulations indicate that the bunch length at the end of the acceleration process is of the order of  $1 \mu\text{m}$  (or less than  $3.3 \text{ fs}$  long), suggesting that attosecond bunches could be produced if the number of electrons injected can be better controlled. The exact conditions for the production of shorter electron bunches using an NA-LWFA scheme could be determined using 3D PIC simulations. If proven to be experimentally realizable, this technique could open up new ways for the development and application of ultrashort radiation sources [4,31,32].

## ACKNOWLEDGMENTS

This work was supported by Institute for Basic Science under IBS-R012-D1. J.H.S., S.K.L., and H.T.K. are partially supported by GIST through ‘Research on Advanced Optical Science and Technology’ grant in 2019.

## APPENDIX

### 1. The gas + nanoparticles target system

The gas jet + nanoparticle target consists of two main parts: the supersonic nozzle and the source of nanoparticles. The supersonic nozzle is a conical *de Laval* type nozzle with 2 mm inlet diameter, 3.9 mm outlet diameter, and  $8^\circ$  semiopening angle. Helium gas is fed into the nozzle through a 2 mm diameter pipe placed sideways (see Fig. 1). The gas target is mounted on a motorized stage that controls the movement of the nozzle in all three spatial directions. To limit the amount of gas released in the chamber during the experiment, the gas is fed through a solenoid valve (Parker Series 9) and operated in pulsed mode with an opening time of 6 ms; the laser pulse interacts with the gas jet 3 ms after valve opening. During the experiment, the gas jet profile is continuously monitored using a Fresnel-type interferometer (not shown here) to ensure that the density profile has a uniform distribution under all experimental conditions.

The bottom part of the nozzle is a removable 2 mm thick aluminum plate fixed with screws. The nanoparticle source is based on laser ablation. The ablation laser (AL), with a wavelength of 532 nm, 3 ns pulse length, and a beam size of 5 mm, is focused down into the gas nozzle and ablates the surface of the removable plate. Previously published results [20] have shown that the ablation plume produced by a nanosecond, picosecond, or femtosecond laser can contain significant amounts of nanoparticles and micron-sized structures. The density and size of nanoparticles generated through laser ablation depend on the laser fluence, laser pulse length, and the type of material ablated. The ablation plume mixes with the helium gas and is transported towards the outlet of the nozzle, where it interacts with the main laser beam. The energy of the AL is empirically set to 10 mJ per pulse, for which the divergence and energy spread of the electron beam is lowest. Under these conditions, the AL fluence on the target is  $10 \text{ J/cm}^2$ , which, according to published works [20,21], creates nanoparticles with sizes on the order of tens of nm. This assumption is confirmed by atomic force microscopy measurements (Figs. 5 and 6), which show that the majority of generated nanoparticles have diameters between 1 nm and 20 nm. Optical probing using interferometry does not show any phase shift when interferograms with and without nanoparticle present are compared, which means that the nanoparticle density is much lower than the sensitivity limit of the interferometer. Using a theoretical estimation based on the amount of ablated material [21] and assuming that all material is transformed into spherical nanoparticles with 20 nm diameter, we obtain

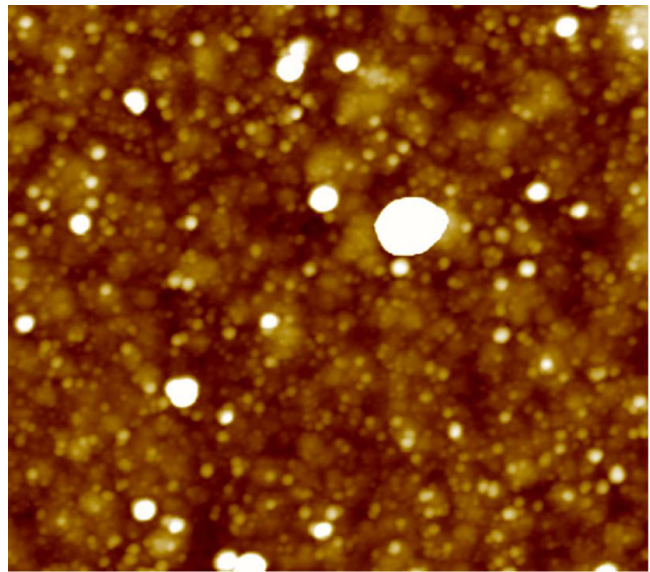


FIG. 5.  $2 \times 2 \mu\text{m}$  surface area AFM image of a sample placed above the nanoparticle source at 15 cm distance from the gas nozzle. The sample accumulated nanoparticles from the entire experiment (around 300 shots).

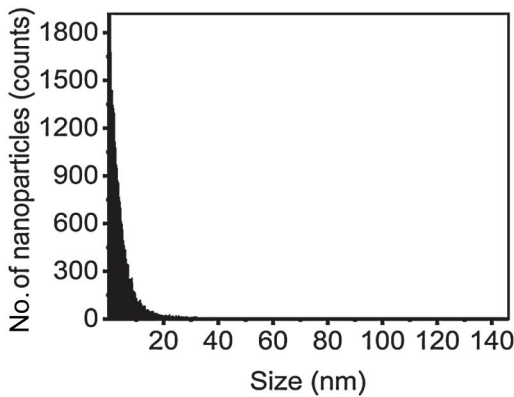


FIG. 6. The distribution of the number of nanoparticles as a function of their sizes. The distribution is obtained by counting the number of nanoparticles from the AFM image.

about  $10^{11}$  nanoparticles per shot. This estimation is based on idealized parameters; thus, the number of nanoparticles is expected to be much lower. By changing the time delay between the ablation laser and the main laser, and monitoring the quality of accelerated electron beam, it is easy to observe that the of the nanoparticles can be seen for approximately  $3 \mu\text{s}$ . Taking into account the gas jet speed, which is supersonic (1000 m/s), we estimate that the nanoparticles are present in a cylindrical volume of 4 mm in diameter and 4.2 mm high. For the sake of simplicity, we ignore the shape of the expanding gas jet. The density of nanoparticles can be approximated to be about  $10^7$ – $10^8$  nanoparticles/cm<sup>3</sup>.

## 2. The laser wakefield accelerator setup

The high-power Ti:sapphire laser, with a central wavelength of 800 nm, p polarization, based on the chirped pulse amplification technique [33], delivers 1.8 J pulses (after compressor) with a temporal duration of  $(27 \pm 2)$  fs at a repetition rate of 5 Hz. A spherical mirror with a focal length of 1 m focuses down the 65 mm in diameter laser beam to a focal spot with a diameter of  $40 \mu\text{m}$  measured at full width at half maximum (FWHM), which contains 60% of the total energy. This ensures, on target, a normalized FWHM vector potential of  $a_0 = 1.07$ .

For the entire experiment, the laser beam is focused at the start of the density ramp, 2 mm longitudinally from the center of the nozzle, with the spot placed horizontally in the center of the gas nozzle and vertically at a distance of 1.5 mm above the nozzle exit. The transverse and longitudinal alignment is done with a top-view imaging setup, consisting of a CCD camera (FLIR BFLY-U3-50H5M-C) equipped with a camera lens (135 mm F2.8) and a BG39 glass filter to cut the scattered light from the laser. The top-view setup is also used to monitor the optical emission from the plasma channel [34,35].

The Lanex 1 setup consists of a  $6 \times 6$  cm Gd<sub>2</sub>O<sub>2</sub>S:Tb screen (Lanex Back) placed at 410 mm from the gas jet and imaged onto a CCD camera with a camera lens (100 mm F2.8), and provides information about the transverse electron profile, pointing, divergence and relative charge. The results for each dataset (taken under the same experimental conditions) are averaged and the mean value and the mean standard error are calculated.

The electron spectrometer (ESPEC) consists of a 0.996 T dipole magnet that has an opening with a height, width, and length of  $8 \times 70 \times 205$  mm<sup>3</sup>. The entrance of the ESPEC is placed at a distance of 455 mm from the gas nozzle and dispersed electrons in the horizontal direction as a function of their energy onto a  $430 \times 80$  mm<sup>2</sup> Gd<sub>2</sub>O<sub>2</sub>S:Tb screen (Lanex Back) placed at 1155 mm from the gas nozzle. The Lanex screen is imaged onto a CCD camera with a lens (16 mm F1.4). The error in energy reading of the electron spectrometer is determined by the electron beam size and pointing and varied depending on energy between +6 MeV and -3.2 MeV for 175 MeV and between +35 MeV and -15.7 MeV for 400 MeV. The energy calibration of the electron spectrometer is done using the G4beamline code [36]. After energy calibration, the peak energy (the part of the energy spectrum that contains most of the charge) is determined from the electron energy with maximum counts in the image.

## 3. Parameters of particle-in-cell simulations

We perform a set of 2D PIC simulations using OSIRIS [24] to illustrate the physics behind the nanoparticle-assisted trapping of electrons in the nonlinear wakefield. A two-dimensional simulation box ( $x$ - $z$ ), moving with velocity  $c$ , is considered with dimensions  $20 \times 60 (c/\omega_p)^2$  divided into  $20\,000 \times 60\,000$  cells. We consider a pre-formed neutral plasma of two species: plasma electrons, initialized with  $4 \times 4$  particles per cell, and nanoparticle electrons, initialized with  $100 \times 100$  particles per cell. For the simulation, we consider a laser with  $a_0 = 3.0$ , FWHM spot diameter  $D_0 = 40 \mu\text{m}$ , and FWHM pulse length  $\tau_0 = 30$  fs, propagating in a preionized plasma with density  $5 \times 10^{18} \text{ cm}^{-3}$ . A preionized, 20 nm in diameter, and  $100n_{\text{cr}}$  in charge density, nanosized plasma is initialized on the laser axis.

We have not run three-dimensional (3D) PIC simulations due to the high grid resolution required to resolve the nanoparticle; this makes the computational cost prohibitive for us. In addition, one can observe that a higher  $a_0$  is used in the 2D simulations, as compared with the experiments. This is done intentionally to match the position of self-injection (without nanoparticle) in 2D simulations with the full-scale 3D simulations taking into account the same laser parameters as those used in the experiments, i.e.,  $a_0 = 1.0$ , FWHM spot diameter  $D_0 = 40 \mu\text{m}$ , and

FWHM pulse length  $\tau_0 = 30$  fs. We observe that in both cases self-injection occurs at a plasma length of 5 mm.

For the 3D (2D) simulations, without the nanoparticle, we consider a moving box, propagating with velocity  $c$ , of dimensions  $20 \times 60 \times 60$  ( $c/\omega_p$ )<sup>3</sup> [ $20 \times 60$  ( $c/\omega_p$ )<sup>2</sup>] divided into  $2000 \times 600 \times 600$  ( $2000 \times 600$ ) cells, and 2 (16) particles per cell for the BPE.

- 
- [1] C. Schroeder, W. Fawley, E. Esarey, and W. Leemans, in *FEL Conf. Proc. TUPPH055* (2006).
- [2] F. Grüner, S. Becker, U. Schramm, T. Eichner, M. Fuchs, R. Weingartner, D. Habs, J. Meyer-Ter-Vehn, M. Geissler, M. Ferrario, L. Serafini, B. Van Der Geer, H. Backe, W. Lauth, and S. Reiche, Design considerations for table-top, laser-based VUV and X-ray free electron lasers, *Appl. Phys. B Lasers Opt.* **86**, 431 (2007).
- [3] V. Malka, J. Faure, and Y. A. Gauduel, Ultra-short electron beams based spatio-temporal radiation biology and radiotherapy, *Mutat. Res. - Rev. Mutat. Res.* **704**, 142 (2010).
- [4] F. Albert and A. G. R. Thomas, Applications of laser wake-field accelerator-based light sources, *Plasma Phys. Control. Fusion* **58**, 103001 (2016).
- [5] A. Pukhov and J. Meyer-ter-Vehn, Laser wake field acceleration: The highly non-linear broken-wave regime, *Appl. Phys. B Lasers Opt.* **74**, 355 (2002).
- [6] W. Lu, C. Huang, M. Zhou, W. B. Mori, and T. Katsouleas, Nonlinear Theory for Relativistic Plasma Wake-fields in the Blowout Regime, *Phys. Rev. Lett.* **96**, 165002 (2006).
- [7] A. Modena, Z. Najmudin, A. E. Dangor, C. E. Clayton, K. A. Marsh, C. Joshi, V. Malka, C. B. Darrow, C. Danzon, D. Neely, and F. N. Walsh, Electron acceleration from the breaking of relativistic plasma waves, *Nature* **377**, 606 (1995).
- [8] S. Kalmykov, S. Yi, V. Khudik, and G. Shvets, Electron Self-Injection and Trapping into an Evolving Plasma Bubble, *Phys. Rev. Lett.* **103**, 135004 (2009).
- [9] E. Esarey, C. Schroeder, and W. Leemans, Physics of laser-driven plasma-based electron accelerators, *Rev. Mod. Phys.* **81**, 1229 (2009).
- [10] J. Faure, C. Rechatin, A. Norlin, A. Lifschitz, Y. Glinec, and V. Malka, Controlled injection and acceleration of electrons in plasma wakefields by colliding laser pulses, *Nature* **444**, 737 (2006).
- [11] H. Kotaki, S. Masuda, M. Kando, J. K. Koga, and K. Nakajima, Head-on injection of a high quality electron beam by the interaction of two laser pulses, *Phys. Plasmas* **11**, 3296 (2004).
- [12] K. Schmid, A. Buck, C. M. S. Sears, J. M. Mikhailova, R. Tautz, D. Herrmann, M. Geissler, F. Krausz, and L. Veisz, Density-transition based electron injector for laser driven wakefield accelerators, *Phys. Rev. Spec. Top. - Accel. Beams* **13**, 091301 (2010).
- [13] H. Suk, N. Barov, J. B. Rosenzweig, and E. Esarey, Plasma Electron Trapping and Acceleration in a Plasma Wake Field Using a Density Transition, *Phys. Rev. Lett.* **86**, 1101 (2001).
- [14] E. Oz, et al., Ionization-Induced Electron Trapping in Ultrarelativistic Plasma Wakes, *Phys. Rev. Lett.* **98**, 084801 (2007).
- [15] A. Pak, K. A. Marsh, S. F. Martins, W. Lu, W. B. Mori, and C. Joshi, Injection and Trapping of Tunnel-Ionized Electrons into Laser-Produced Wakes, *Phys. Rev. Lett.* **104**, 025003 (2010).
- [16] J. Vieira, S. F. Martins, V. B. Pathak, R. A. Fonseca, W. B. Mori, and L. O. Silva, Magnetic Control of Particle Injection in Plasma Based Accelerators, *Phys. Rev. Lett.* **106**, 225001 (2011).
- [17] B. Shen, Y. Li, K. Nemeth, H. Shang, Y. C. Chae, R. Soliday, R. Crowell, E. Frank, W. Groppe, and J. Cary, Electron injection by a nanowire in the bubble regime, *Phys. Plasmas* **14**, 053115 (2007).
- [18] M. H. Cho, V. B. Pathak, H. T. Kim, and C. H. Nam, Controlled electron injection facilitated by nanoparticles for laser wakefield acceleration, *Sci. Rep.* **8**, 16924 (2018).
- [19] P. Liu, P. J. Ziemann, D. B. Kittelson, and P. H. McMurry, Generating particle beams of controlled dimensions and divergence. 2. Experimental evaluation of particle motion in aerodynamic lenses and nozzle expansions, *Aerosol Sci. Technol.* **22**, 314 (1995).
- [20] M. Kim, S. Osone, T. Kim, H. Higashi, and T. Seto, Synthesis of nanoparticles by laser ablation: A review, *KONA Powder Part. J.* **34**, 80 (2017).
- [21] K. H. Leitz, B. Redlingshöfer, Y. Reg, A. Otto, and M. Schmidt, Metal ablation with short and ultrashort laser pulses, *Phys. Procedia* **12**, 230 (2011).
- [22] M. Tzoufras, W. Lu, F. Tsung, C. Huang, W. Mori, T. Katsouleas, J. Vieira, R. Fonseca, and L. Silva, Beam Loading in the Nonlinear Regime of Plasma-Based Acceleration, *Phys. Rev. Lett.* **101**, 145002 (2008).
- [23] C. Rechatin, X. Davoine, A. Lifschitz, A. Ben Ismail, J. Lim, E. Lefebvre, J. Faure, and V. Malka, Observation of Beam Loading in a Laser-Plasma Accelerator, *Phys. Rev. Lett.* **103**, 194804 (2009).
- [24] R. A. Fonseca, L. O. Silva, F. S. Tsung, V. K. Decyk, W. Lu, C. Ren, W. B. Mori, S. Deng, S. Lee, T. C. Katsouleas, and J. C. Adam, in *Int. Conf. Comput. Sci., Part III* (2002), p. 342.
- [25] C. D. Decker, W. B. Mori, K. C. Tzeng, and T. Katsouleas, The evolution of ultra-intense, short-pulse lasers in underdense plasmas, *Phys. Plasmas* **3**, 2047 (1996).
- [26] E. Brunetti, R. P. Shanks, G. G. Manahan, M. R. Islam, B. Ersfeld, M. P. Anania, S. Cipiccia, R. C. Issac, G. Raj, G. Vieux, G. H. Welsh, S. M. Wiggins, D. A. Jaroszynski, and Low Emittance, High Brilliance Relativistic Electron Beams from a Laser-Plasma Accelerator, *Phys. Rev. Lett.* **105**, 215007 (2010).
- [27] S. Banerjee, N. D. Powers, V. Ramanathan, I. Ghebregziabher, K. J. Brown, C. M. Maharjan, S. Chen, A. Beck, E. Lefebvre, S. Y. Kalmykov, B. A. Shadwick, and D. P. Umstadter, Generation of tunable, 100-800 MeV quasi-monoenergetic electron beams from a laser-wakefield accelerator in the blowout regime, *Phys. Plasmas* **19**, 056703 (2012).
- [28] X. Wang, et al., Quasi-monoenergetic laser-plasma acceleration of electrons to 2 GeV, *Nat. Commun.* **4**, 1988 (2013).

- [29] S. M. Wiggins, R. C. Issac, G. H. Welsh, E. Brunetti, R. P. Shanks, M. P. Anania, S. Cipiccia, G. G. Manahan, C. Aniculaesei, B. Ersfeld, M. R. Islam, R. T. L. Burgess, G. Vieux, W. A. Gillespie, A. M. MacLeod, S. B. Van Der Geer, M. J. De Loos, and D. A. Jaroszynski, High quality electron beams from a laser wakefield accelerator, *Plasma Phys. Control. Fusion* **52**, 124032 (2010).
- [30] D. Gustas, D. Guénöt, A. Vernier, S. Dutt, F. Böhle, R. Lopez-Martens, A. Lifschitz, and J. Faure, High-charge relativistic electron bunches from a kHz laser-plasma accelerator, *Phys. Rev. Accel. Beams* **21**, 013401 (2018).
- [31] H.-P. Schlenvoigt, K. Haupt, A. Debus, F. Budde, O. Jäckel, S. Pfotenhauer, H. Schwoerer, E. Rohwer, J. G. Gallacher, E. Brunetti, R. P. Shanks, S. M. Wiggins, and D. A. Jaroszynski, A compact synchrotron radiation source driven by a laser-plasma wakefield accelerator, *Nat. Phys.* **4**, 130 (2007).
- [32] D. A. Jaroszynski, R. Bingham, E. Brunetti, B. Ersfeld, J. Gallacher, B. Van Der Geer, R. Issac, S. P. Jamison, D. Jones, M. De Loos, A. Lyachev, V. Pavlov, A. Reitsma, Y. Saveliev, G. Vieux, and S. M. Wiggins, Radiation sources based on laser-plasma interactions, *Philos. Trans. R. Soc. A Math. Phys. Eng. Sci.* **364**, 20051732 (2006).
- [33] D. Strickland and G. Mourou, Compression of amplified chirped optical pulses, *Opt. Commun.* **56**, 219 (1985).
- [34] E. Esarey, S. K. Ride, and P. Sprangle, Nonlinear Thomson scattering of intense laser pulses from beams and plasmas, *Phys. Rev. E* **48**, 3003 (1993).
- [35] S. Y. Chen, A. Maksimchuk, and D. Umstadter, Experimental observation of relativistic nonlinear Thomson scattering, *Nature* **396**, 653 (1998).
- [36] T. J. Roberts and D. M. Kaplan, in *Proc. IEEE Part. Accel. Conf.* (2007), p. 3468.